Experimental verification of optical models of graphene with multimode slab waveguides

CHANG, Zeshan; CHIANG, Kin Seng

Published in:
Optics Letters

Published: 01/05/2016

Document Version:
Post-print, also known as Accepted Author Manuscript, Peer-reviewed or Author Final version

Published version (DOI):
10.1364/OL.41.002129

Publication details:
CHANG, Z., & CHIANG, K. S. (2016). Experimental verification of optical models of graphene with multimode slab waveguides. *Optics Letters*, *41*(9), 2129-2132. Advance online publication. https://doi.org/10.1364/OL.41.002129

Experimental verification of optical models of graphene with multimode slab waveguides

ZESHAN CHANG, KIN SENG CHIANG*

Department of Electronic Engineering, City University of Hong Kong, Hong Kong, China
**Corresponding author: eeksc@cityu.edu.hk*

Received XX Month XXXX; revised XX Month, XXXX; accepted XX Month XXXX; posted XX Month XXXX (Doc. ID XXXXX); published XX Month XXXX

We compare three optical models of graphene, namely the interface model, the isotropic model, and the anisotropic model, and verify them experimentally with two multimode slab waveguide samples operating at the wavelengths 632.8 nm and 1536 nm. By comparing the calculated graphene-induced losses and the measurement data, we confirm that the interface model and the anisotropic model give correct results for both the transverse electric (TE) and transverse magnetic (TM) modes, while the isotropic model gives correct results only for the TE modes. With the experimental data, we also quantitatively verify the widely used expression for the surface conductivity of graphene in the optical regime. Our findings clarify the issue of modeling graphene in the analysis of graphene-incorporated waveguides and offer deeper insight into the optical properties of graphene for waveguide applications.

OCIS codes: *(130.2790) Guided waves; (130.3130) Integrated optics materials; (260.2110) Electromagnetic optics; (310.6860) Thin films, optical properties.*

http://dx.doi.org/10.1364/OL.99.099999

Graphene, a two-dimensional (2D) single layer of carbon atoms, possesses many useful optical properties, such as electrically tunable absorption, exceptionally strong nonlinearity, saturable absorption, and efficient luminescence [1-7], and promises many interesting applications in the field of photonics. By incorporating graphene films into optical waveguide structures, in particular, effective guided-wave devices, such as electrically tunable optical modulators [5-8], broadband optical polarizers [9-12], and optical sensors [13], can be realized.

In the analysis of graphene-incorporated optical waveguides, the interface model [7-9] and the isotropic model [6,13-18] are commonly used. In the interface model, graphene is treated as a pure conductivity boundary with no thickness, while in the isotropic model, it is treated as an isotropic medium with an equivalent complex relative permittivity and a finite thickness (customarily set at 1 nm) [15-18]. The isotropic model is simple to apply and more widely used in practical applications, especially for complicated geometric structures. However, graphene being a 2D structure, there should be no volume current along the direction perpendicular to its surface, which means that its equivalent relative permittivity should not be isotropic. Graphene may rather be considered as an anisotropic material [19-24] characterized by a relative permittivity tensor. The primary objective of our study is to compare these models with both numerical and experimental results for multimode slab waveguides. The slab waveguides we use can provide accurate measurement data for different modes and different wavelengths, which can sharply differentiate the models. Our study confirms that the interface model and the anisotropic model give correct results for graphene-induced losses for both the transverse-electric (TE) and transverse-magnetic (TM) modes, while the isotropic model gives correct results only for the TE modes. The close agreement between the calculated results and the experimental data also quantitatively verifies the widely used expression [25] for the surface conductivity of graphene in the optical regime. Our study clarifies the performances of various models of graphene in waveguide analysis and consolidates the theoretical basis of modeling graphene in the optical regime.

In the interface model, a graphene film is considered as a conductive surface with conductivity σ and zero thickness, which causes a surface current and hence a discontinuous magnetic field across the boundary. To the best of our knowledge, this model has been applied to only simple slab waveguide structures [7-9].

In the isotropic model, a graphene film is assumed to possess a finite thickness Δ and a volume conductivity σ/Δ, which gives a volume current density $\boldsymbol{J} = \sigma/\Delta \times \boldsymbol{E}$, where $\boldsymbol{E}$ is the electric field. For an electromagnetic wave oscillating at a radian frequency ω, one finds, from the Maxwell equation, $\nabla \times \boldsymbol{H} = \boldsymbol{J} - j\omega\varepsilon_0\boldsymbol{E} = -j\omega\varepsilon_0[1 + j\sigma/(\omega\varepsilon_0\Delta)]\boldsymbol{E}$, where ε_0 is the permittivity of vacuum and j is the imaginary unit, which thus leads to the definition of an equivalent isotropic relative permittivity for the graphene film:

$$\varepsilon_g(\omega) = 1 + \frac{j\sigma}{\omega\varepsilon_0\Delta}, \tag{1}$$

where the second term represents the effect of the volume current. However, as graphene is a 2D structure, there should be no volume

current in the direction perpendicular to the surface of the graphene film (the normal direction). The equivalent relative permittivity given by Eq. (1) is valid only in the direction parallel to the surface (the tangential direction). Therefore, the model should be valid only for the TE wave that has a single electric-field component in the tangential direction, and should not be valid for the TM wave that has a strong electric-field component in the normal direction. Nevertheless, the isotropic model has been widely applied to various optical waveguide structures [6,13-18].

In the anisotropic model, the volume current in the normal direction is removed, which thus leads to the following relative permittivity tensor for graphene:

$$\hat{\varepsilon}_g = \begin{bmatrix} 1 & 0 & 0 \\ 0 & \varepsilon_g & 0 \\ 0 & 0 & \varepsilon_g \end{bmatrix}. \quad (2)$$

The anisotropic model has recently been used in the analysis of surface plasmon polariton waveguides in the mid-infrared and THz regimes [19-24], where the real part of the relative permittivity of graphene is taken as 2.5 (the value of graphite) [20-24] or the real part of the tangential elements is taken as 1.0, but the normal element is taken as 2.5 [19]. Even in some studies using the isotropic model [17,18], the real part of the relative permittivity of graphene is totally ignored (i.e., set to zero). Here, to be consistent with the model given by Eq. (1) [14], we use the value 1.0. Physically, graphene consists of only a single atom layer and the dipole induced in the normal direction by the propagating electromagnetic wave should be weak, so its out-of-plane relative permittivity may be taken as that of vacuum (i.e., 1.0). In fact, because the graphene film is extremely thin (of the order of 1 nm), compared with the mode size (a few μm), the real part of its relative permittivity, whether taking the value 1.0 or 2.5, has little effect on the effective index and the mode field distribution.

The most important parameter involved in all these models is the conductivity of graphene σ, which is approximated by the following expression [25]:

$$\sigma(\omega) = \frac{je^2\mu_c}{\pi\hbar^2(\omega + j\tau^{-1})} + \frac{je^2}{4\pi\hbar}\ln\left[\frac{2|\mu_c| - (\omega + j\tau^{-1})\hbar}{2|\mu_c| + (\omega + j\tau^{-1})\hbar}\right], \quad (3)$$

where μ_c = 0.3 eV is the chemical potential, $\tau = 5 \times 10^{-13}$ s is the relaxation time, $\hbar = h/2\pi$ is the reduced Planck's constant, and e is the electron charge. The two terms in Eq. (3) represent, respectively, the intraband and interband contributions from the Kubo formula. While Eq. (3) has been widely quoted in the literature [7-11,13,15,16], there has been no experimental verification of its accuracy in the optical regime.

To compare the three models, we consider two graphene-embedded multimode slab waveguides, as shown schematically in Fig. 1(a) and Fig. 1(b), respectively, where the guided waves are confined in the x direction and propagate in the z direction. For the waveguide in Fig. 1(a) (Structure 1), the graphene film is embedded inside the core layer, while for the waveguide in Fig. 1(b) (Structure 2), the graphene film is embedded between the core and the cladding layer. These waveguides support pure TE and TM modes and can provide accurate measurement data to verify the models. Our task is to calculate the effective indices of the guided TE and TM modes of the waveguides and compare the calculated results with measurements obtained from experimental waveguide samples. Because of the presence of the conductivity (or the complex relative permittivity), the modes in general have complex effective indices n_{eff}. The modal loss is related to the imaginary part of the effective index by $10\log_{10}\{\exp[2k_0\,\mathrm{Im}(n_{eff})]\} = 8.68\,k_0\,\mathrm{Im}(n_{eff})$ (in dB per unit length of the waveguide), where $k_0 = 2\pi/\lambda$ is the free-space wavenumber with λ being the free-space wavelength.

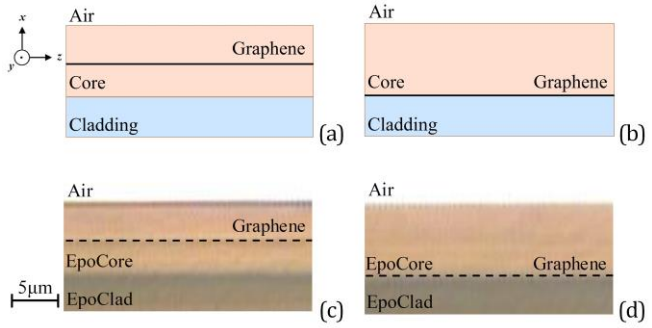

Fig. 1. Schematic diagrams of slab waveguides with graphene embedded (a) in the core layer (Structure 1) and (b) between the core and the cladding layer (Structure 2), and photographs of the fabricated samples for (c) Structure 1 and (d) Structure 2.

In applying the interface model, the graphene film is treated as a conductive boundary condition, namely $\boldsymbol{H}_1 - \boldsymbol{H}_2 = \sigma \times \boldsymbol{E}$, where $\boldsymbol{H}_1$ and $\boldsymbol{H}_2$ are the tangential magnetic fields on the two sides of graphene, respectively. The TE and TM dispersion equations are obtained by solving the corresponding wave equations subject to the boundary conditions across different layers of the structure [9, 26]. The effective indices of the modes are then solved from the dispersion equations by using a root-searching algorithm.

In applying the isotropic model and the anisotropic model, the graphene film is assumed to have a thickness of 1 nm. The multi-layer waveguide structure is solved by the transfer matrix method, where each layer is represented by a 2 × 2 matrix and the dispersion equations are obtained by multiplying the matrices of all layers [27]. The transfer matrix method can accommodate both lossy and anisotropic media.

For the experimental work, we fabricated the two waveguide structures by the standard spin-coating process with the polymer materials EpoCore and EpoClad (Micro Resist Technology) as the core and cladding materials, respectively [28]. The refractive indices of the EpoCore and EpoClad films, measured with a commercial prism-coupler system (Metricon 2010), were 1.594 (1.572) and 1.580 (1.558), respectively, at the wavelength 632.8 (1536) nm, which were insensitive to the polarization of light. For both structures, the cladding layer was coated on a Si wafer to a thickness of ~13 μm. For Structure 1, the core layer had a thickness of 9.0 μm and a graphene film was embedded in the core layer at a distance of 4.1 μm from the cladding layer. For Structure 2, the core layer also had a thickness of 9.0 μm and a graphene film was embedded between the core and the cladding layer. The mono-atom graphene film used (Hefei Vigon Tech.) had a dimension of 10 ×10 mm^2, which came as an attachment to a PMMA buffer. To transfer the graphene film onto the waveguide, the buffer was floated to deionized water and fished by the waveguide sample. The PMMA buffer was then dried and removed from the waveguide by acetone. The area of the sample that was not covered by the graphene film was used as the reference waveguide. The lengths of the waveguide samples were about 20

mm. Photographs of the waveguide samples for Structure 1 and Structure 2 are shown in Fig. 1(c) and Fig. 1(d), respectively.

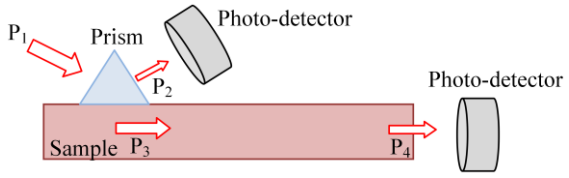

Fig. 2. Setup of the prism-coupler method for the characterization of the slab waveguide sample.

We employed the commercial prism-coupler system to measure the effective indices (real part) and the propagation losses of the modes. The measurement setup is shown schematically in Fig. 2. A collimated laser beam with power P_1 is incident upon a high-index prism placed against the waveguide sample. The polarization state of the laser beam can be controlled to select the TE or the TM polarization. Each guided mode of the waveguide can be selectively excited with a specific incidence angle that satisfies the phase-matching condition and the real part of the effective index of the excited mode can be determined by scanning the incidence angle. The output power from the prism, denoted as P_2, is measured with a photo-detector. The power coupled into the mode of the waveguide can be approximated by $P_3 = P_1 - P_2$. The output power from the waveguide, denoted as P_4, is also measured with a photo-detector. The propagation loss of the excited mode is obtained by $P_3 - P_4 = P_1 - P_2 - P_4$. We measured the propagation losses for the samples with graphene and the reference waveguides without graphene at the wavelengths 632.8 nm and 1536 nm. By subtracting the propagation loss of the sample without graphene from that of the sample with graphene for the same mode, we can determine the loss induced by graphene only. The subtraction also removes common losses due to reflections from the surfaces of the prism and the end face of the waveguide.

Both waveguide samples support 6 TE and 6 TM modes at 632.8 nm and 2 TE and 2 TM modes at 1536 nm. The measured effective indices (real part) for the two samples are shown in Table 1. The values calculated by the three models using the parameters of the fabricated waveguide samples agree closely with the measured values. Our numerical results for waveguides with and without graphene show negligible differences ($<10^{-4}$) in the effective indices (real part), which is also confirmed by our measurements on waveguide samples with and without graphene. While the graphene film has insignificant effects on the effective indices (real part), it has a strong effect on the propagation loss.

Table 1. The measured effective indices (real part)

Mode	Structure 1 at 633 nm	Structure 1 at 1550 nm	Structure 2 at 633 nm	Structure 2 at 1550 nm
TE_0	1.5927	1.5702	1.5927	1.5703
TE_1	1.5910	1.5653	1.5909	1.5653
TE_2	1.5897		1.5894	
TE_3	1.5874		1.5872	
TE_4	1.5849		1.5845	
TE_5	1.5814		1.5810	
TM_0	1.5923	1.5696	1.5922	1.5697
TM_1	1.5904	1.5647	1.5904	1.5647
TM_2	1.5890		1.5888	
TM_3	1.5868		1.5866	
TM_4	1.5842		1.5839	
TM_5	1.5808		1.5805	

Table 2. Propagation losses for Structure 1 at 632.8 nm

Mode	Experiment (dB/cm)	Interface (dB/cm)	Anisotropic (dB/cm)	Isotropic (dB/cm)
TE_0	>23	111	111	111
TE_1	2.2	1.95	1.95	1.95
TE_2	>23	123	123	123
TE_3	5.8	6.22	6.22	6.22
TE_4	>23	118	118	118
TE_5	5.2	4.72	4.72	4.72
TM_0	0.1	0.00489	0.00489	151
TM_1	0.5	0.226	0.226	1.80
TM_2	0.2	0.0199	0.0199	130
TM_3	1.0	0.862	0.862	5.68
TM_4	0.9	0.0649	0.0649	122
TM_5	1.8	1.68	1.68	4.35

Table 3. Propagation losses for Structure 1 at 1536 nm

Mode	Experiment (dB/cm)	Interface (dB/cm)	Anisotropic (dB/cm)	Isotropic (dB/cm)
TE_0	>23	120	120	120
TE_1	1.0	0.889	0.889	0.889
TM_0	0.1	0.00153	0.00153	22.4
TM_1	1.2	1.04	1.04	1.34

Table 4. Propagation losses for Structure 2 at 632.8 nm

Mode	Experiment (dB/cm)	Interface (dB/cm)	Anisotropic (dB/cm)	Isotropic (dB/cm)
TE_0	4.2	3.99	3.99	3.99
TE_1	14	15.8	15.8	15.8
TE_2	>23	35.0	35.0	35.0
TE_3	>23	60.6	60.6	60.6
TE_4	>23	90.0	90.0	90.0
TE_5	>23	110	110	110
TM_0	0.2	0.0488	0.0488	3.99
TM_1	0.5	0.182	0.182	15.8
TM_2	0.6	0.359	0.359	35.0
TM_3	0.6	0.505	0.505	60.6
TM_4	0.5	0.504	0.504	90.0
TM_5	0.2	0.163	0.163	110

Table 5. Propagation losses for Structure 2 at 1536 nm

Mode	Experiment (dB/cm)	Interface (dB/cm)	Anisotropic (dB/cm)	Isotropic (dB/cm)
TE_0	15	14.7	14.7	14.7
TE_1	>23	56.4	56.4	56.4
TM_0	0.2	0.237	0.237	3.11
TM_1	0.3	0.538	0.538	11.2

The graphene-induced propagation losses for the modes in Structure 1 at 632.8 nm and 1536 nm are listed in Table 2 and 3, respectively. The experiment data in the tables are the mean measured values. The uncertainties in the measured propagation losses of the waveguides are typically ±0.4 to 0.5 dB/cm. Note that the maximum graphene-induced loss that could be measured with

our setup was limited to ~23 dB/cm. As shown in Table 2 and Table 3, for the TE modes, the losses calculated by the three models are identical and agree well with the experimental data. The even TE modes (the TE_0, TE_2, and TE_4 modes) suffer from much higher losses than the odd TE modes (the TE_1, TE_3, and TE_5 modes). The reason is that, for Structure 1, the graphene film is located near the middle of the core layer, where the electric fields of the even modes are much stronger than those of the odd modes. As a result, the graphene film, because of its large conductivity, attenuates the even modes much more strongly. For the TM modes, the losses calculated by the interface model and the anisotropic model are identical and agree well with the experimental data. The isotropic model, however, can overestimate the losses of the TM modes (especially the even TM modes) by orders of magnitude.

The graphene-induced propagation losses for the modes in Structure 2 at 632.8 nm and 1536 nm are listed in Table 4 and 5, respectively. Again, for the TE modes, the three models produce the same results, which agree with the experimental data. Because the graphene film is placed at the core-cladding boundary, the odd TE modes can suffer from higher losses than the even TE modes, depending on the magnitude of the electric field at the core-cladding boundary. For the TM modes, the interface model and the anisotropic model give the same results, which agree closely with the experimental data, whereas the isotropic model produces much larger values.

Both examples show that the TE modes suffer from much higher losses than the TM modes, which is the operation principle of the many demonstrated graphene-based waveguide polarizers. Our results also indicate the possibility of achieving large differential losses among modes of different orders, which could be explored as a mechanism of realizing mode-dependent loss compensators and mode filters. The close agreement between the numerical and experimental data with two different structures and two different wavelengths also confirms the high accuracy of Eq. (3) and the associated values for the chemical potential and the relaxation time for the calculation of the conductivity of graphene in the optical regime.

In the isotropic and anisotropic models, monolayer graphene is treated as bulk material with a finite thickness, which has been taken as 1 nm [15-19], 0.5 nm [21,24], or 0.34 nm (the measured thickness of graphene) [2,11,22]. For the TE modes, the losses calculated by both models are accurate and insensitive to the graphene thickness assumed. For the TM modes, however, the losses calculated by the isotropic model are sensitive to the graphene thickness with errors increasing rapidly with the graphene thickness; the use of 0.34 nm still generates large errors. On the other hand, the TM losses calculated by the anisotropic model are insensitive to the graphene thickness, which is consistent with the study in Ref. 24. We find that the anisotropic model produces accurate results even with a graphene thickness as large as 10 nm, which is just another indication of the validity of the anisotropic model.

In summary, we have compared three optical models of graphene (the interface model, the isotropic model, and the anisotropic model) with experimental data obtained from two multimode slab waveguides. By comparing calculated and measured graphene-induced losses, we confirm that the interface model and the anisotropic model give correct results for both the TE and TM modes, while the more popular isotropic model gives correct results only for the TE modes. For more complicated structures, such as channel waveguides and circular fibers, where the modes in general contain electric-field components in three directions, it is necessary to use the interface model or the anisotropic model to produce correct results. The isotropic model is likely to give large errors for such structures. Our experimental data obtained at the wavelengths 632.8 nm and 1536 nm have also quantitatively verified the widely used expression for the calculation of the surface conductivity of graphene in the optical regime, i.e., Eq. (3), which is important for consolidating the understanding of the optical properties of graphene.

Funding. Research Grants Council, University Grants Committee, Hong Kong (CityU 11202014).

REFERENCES

1. F. Bonaccorso, Z. Sun, T. Hasan, and A. C. Ferrari, Nat. Photonics **4**, 611 (2010).
2. W. Zhao, K. Shi, and Z. Lu, Opt. Lett. **38**, 4342 (2013).
3. Z. Sun, T. Hasan, F. Torrisi, D. Popa, G. Privitera, F. Wang, F. Bonaccorso, D. M. Basko, and A. C. Ferrari, ACS Nano **4,** 803 (2010).
4. Z. Luo, M. Zhou, D. Wu, C. Ye, J. Weng, J. Dong, H. Xu, Z. Cai, and L. Chen, J. Lightwave Technol. **29**, 2732 (2011).
5. M. Liu, X. Yin, E. Ulin-Avila, B. Geng, T. Zentgraf, L. Ju, F. Wang, and X. Zhang, Nature **474** , 64 (2011).
6. L. Yang, T. Hu, R. Hao, C. Qui, C. Xu, H. Yu, Y. Xu, X. Jiang, Y. Li, and J. Yang, Opt. Lett. **38**, 2512 (2013).
7. D. A. Kuzmin, I. V. Bychkov, and V. G. Shavrov, Opt. Lett. **40**, 2557 (2015).
8. C. Xu, Y. Jin, L. Yang, J. Yang, and X. Jiang, Opt. Express **20**, 22398 (2012).
9. Q. Bao, H. Zhang, B. Wang, Z. Ni, C. H. Y. X. Lim, Y. Wang, D. Y. Tang, and K. P. Loh, Nat. Photonics **5**, 411 (2011).
10. I. Degli-Eredi, J. E. Sipe, and N. Vermeulen, Opt. Lett. **40**, 2076 (2015).
11. X. Yin, T. Zhang, L. Chen, and X. Li, Opt. Lett. **40**, 1733 (2015).
12. C. Guan, S. Li, Y. Shen, T. Yuan, J. Yang, and L. Yuan, J. Lightwave Technol. **33,** 349 (2015).
13. Y. Wu, B. Yao, A. Zhang, Y. Rao, Z. Wang, Y. Cheng, Y. Gong, W. Zhang, Y. Chen, and K. S. Chiang, Opt. Lett. **39**, 1235 (2014).
14. A. Vakil and N. Engheta, Science **332**, 1291 (2011).
15. B. Wang, X .Zhang, X. Yuan, and J. Teng, Appl. Phys. Lett. **100**, 131111 (2012).
16. H. Lin, M. F. Pantoja, L. D. Angulo, J. Alvarez, R. G. Martin, and S. G. Garcia, IEEE Microw. Wirel. Compon. Lett. **22**, 612 (2012).
17. Y. Jiang, W. B. Lu, H. J. Xu, Z. G. Dong, and T. J. Cui, Phys. Lett. A **376**, 1468 (2012)..
18. H. J. Xu, W. B. Lu, W. Zhu, Z. G. Dong, and T. J. Cui, Appl. Phys. Lett. **100**, 243110 (2012).
19. L. Wang, W. Li, and X. Jiang, Opt. Lett. **40**, 2325 (2015).
20. J. Lao, J. Tao, Q. J. Wang, and X. G. Huang, Laser Photonics Rev. **8**, 569 (2014).
21. J. Liu, X. Zhai, L. Wang, H. Li, F. Xie, S. Xia, X. Shang, and X. Luo, Opt. Express **24**, 5376 (2016).
22. S. Xia, X. Zhai, L. Wang, Q. Lin, and S. Wen, Opt. Express **24**, 427 (2016).
23. L. A. Falkovsky, J. Phys: Conf. Ser. **129**, 012004 (2008).
24. W. Gao, J. Shu, C. Qui, and Q. Xu, ACS Nano **6**, 7806 (2012).
25. S. A. Mikhaillov and K. Ziegler, Phys. Rev. Lett. **99**, 016803 (2007).
26. K. Okamoto, *Fundamentals of optical waveguides* (Academic Press, San Diego, 2000).
27. C. Chen, P. Berini, D. Feng, S. Tanev, and V. P. Tzolov, Opt. Express **7**, 260 (2000).
28. J. Dong, K. S. Chiang, and W. Jin, Opt. Lett. **40**, 3125 (2015).

Full References

1. F. Bonaccorso, Z. Sun, T. Hasan, and A. C. Ferrari, "Graphene photonics and optoelectronics," Nat. Photonics **4**, 611 (2010).
2. W. Zhao, K. Shi, and Z. Lu, "Greatly enhanced ultrabroadband light absorption by monolayer graphene," Opt. Lett. **38**, 4342 (2013).
3. Z. Sun, T. Hasan, F. Torrisi, D. Popa, G. Privitera, F. Wang, F. Bonaccorso, D. M. Basko, and A. C. Ferrari, "Graphene mode-locked ultrafast laser," ACS Nano **4,** 803 (2010).
4. Z. Luo, M. Zhou, D. Wu, C. Ye, J. Weng, J. Dong, H. Xu, Z. Cai, and L. Chen, "Graphene-induced nonlinear four-wave-mixing and its application to multiwavelength Q-switched rare-earth-doped fiber lasers," J. Lightwave Technol. **29**, 2732 (2011).
5. M. Liu, X. Yin, E. Ulin-Avila, B. Geng, T. Zentgraf, L. Ju, F. Wang, and X. Zhang, "A graphene-based broadband optical modulator," Nature **474** , 64 (2011).
6. L. Yang, T. Hu, R. Hao, C. Qui, C. Xu, H. Yu, Y. Xu, X. Jiang, Y. Li, and J. Yang, "Low-chirp high-extinction-ratio modulator based on graphene-silicon waveguide," Opt. Lett. **38**, 2512 (2013).
7. D. A. Kuzmin, I. V. Bychkov, and V. G. Shavrov, "Magnetic field control of plasmon polaritons in graphene-covered gyrotropic planar waveguide," Opt. Lett. **40**, 2557 (2015).
8. C. Xu, Y. Jin, L. Yang, J. Yang, and X. Jiang, "Characteristics of electro-refractive modulating based on graphene-oxide-silicon waveguide," Opt. Express **20**, 22398 (2012).
9. Q. Bao, H. Zhang, B. Wang, Z. Ni, C. H. Y. X. Lim, Y. Wang, D. Y. Tang, and K. P. Loh, "Broadband graphene polarizer," Nat. Photonics **5**, 411 (2011).
10. I. Degli-Eredi, J. E. Sipe, and N. Vermeulen, "TE-polarized graphene modes sustained by photonic crystal structures," Opt. Lett. **40**, 2076 (2015).
11. X. Yin, T. Zhang, L. Chen, and X. Li, "Ultra-compact TE-pass polarizer with graphene multilayer embedded in a silicon slot waveguide," Opt. Lett. **40**, 1733 (2015).
12. C. Guan, S. Li, Y. Shen, T. Yuan, J. Yang, and L. Yuan, "Graphene-coated surface core fiber polarizer," J. Lightwave Technol. **33 ,** 349 (2015).
13. Y. Wu, B. Yao, A. Zhang, Y. Rao, Z. Wang, Y. Cheng, Y. Gong, W. Zhang, Y. Chen, and K. S. Chiang, "Graphene-coated microfiber Bragg grating for high sensitivity gas sensing," Opt. Lett. **39**, 1235 (2014).
14. A. Vakil and N. Engheta, "Transformation optics using graphene," Science **332**, 1291 (2011).
15. B. Wang, X .Zhang, X. Yuan, and J. Teng, "Optical coupling of surface plasmons between graphene sheets," Appl. Phys. Lett. **100**, 131111 (2012).
16. H. Lin, M. F. Pantoja, L. D. Angulo, J. Alvarez, R. G. Martin, and S. G. Garcia, "FDTD modeling of graphene devices using complex conjugate dispersion material model," IEEE Microw. Wirel. Compon. Lett. **22**, 612 (2012).
17. Y. Jiang, W. B. Lu, H. J. Xu, Z. G. Dong, and T. J. Cui, "A planar electromagnetic 'black hole' based on graphene," Phys. Lett. A **376**, 1468 (2012).
18. H. J. Xu, W. B. Lu, W. Zhu, Z. G. Dong, and T. J. Cui, "Efficient manipulation of surface plasmon polariton waves in graphene," Appl. Phys. Lett. **100**, 243110 (2012).
19. L. Wang, W. Li, and X. Jiang, "Tunable control of electromagnetically induced transparency analogue in a compact graphene-based waveguide," Opt. Lett. **40**, 2325 (2015).
20. J. Lao, J. Tao, Q. J. Wang, and X. G. Huang, " Tunable graphene-based plasmonic waveguides: nano modulators and nano attenuators," Laser Photonics Rev. **8**, 569 (2014).
21. J. Liu, X. Zhai, L. Wang, H. Li, F. Xie, S. Xia, X. Shang, and X. Luo, "Graphene-based long-range SPP hybrid waveguide with ultra-long propagation length in mid-infrared range," Opt. Express **24**, 5376 (2016).
22. S. Xia, X. Zhai, L. Wang, Q. Lin, and S. Wen, "Excitation of crest and trough surface plasmon modes in in-plane bended graphene nanoribbons," Opt. Express **24**, 427 (2016).
23. L. A. Falkovsky, "Optical properties of graphene," J. Phys: Conf. Ser. **129**, 012004 (2008).
24. W. Gao, J. Shu, C. Qui, and Q. Xu, "Excitation of plasmonic waves in graphene by guided-mode resonances," ACS Nano **6**, 7806 (2012).
25. S. A. Mikhaillov and K. Ziegler, "A new electromagnetic mode in graphene," Phys. Rev. Lett. **99**, 016803 (2007).
26. K. Okamoto, *Fundamentals of optical waveguides* (Academic Press, San Diego, 2000).
27. C. Chen, P. Berini, D. Feng, S. Tanev, and V. P. Tzolov, "Efficient and accurate numerical analysis of multilayer planar optical waveguides in lossy anisotropic media," Opt. Express **7**, 260 (2000).
28. J. Dong, K. S. Chiang, and W. Jin, "Mode multiplexer based on integrated horizontal and vertical polymer waveguide couplers," Opt. Lett. **40**, 3125 (2015).